buildings

MDPI

Article

# Artificial Neural Network Estimation of the Effect of Varying Curing Conditions and Cement Type on Hardened Concrete Properties

**Gökhan Kaplan [1,*], Hasbi Yaprak [1], Selçuk Memiş [1] and Abdoslam Alnkaa [2]**

[1] Department of Civil Engineering, Faculty of Engineering and Architecture, Kastamonu University, 37150 Kastamonu, Turkey; hyaprak@kastamonu.edu.tr (H.Y.); smemis@kastamonu.edu.tr (S.M.)
[2] Departmentof Materials Science and Engineering, Institute of Science, Kastamonu University, 37150 Kastamonu, Turkey; nankaa@rocketmail.com
* Correspondence: gkaplan@kastamonu.edu.tr; Tel.: +90-366-280-2959

Received: 28 November 2018; Accepted: 19 December 2018; Published: 3 January 2019

check for updates

**Abstract:** The use of mineral admixtures and industrial waste as a replacement for Portland cement is recognized widely for its energy efficiency along with reduced $CO_2$ emissions. The use of materials such as fly ash, blast-furnace slag or limestone powder in concrete production makes this process a sustainable one. This study explored a number of hardened concrete properties, such as compressive strength, ultrasonic pulse velocity, dynamic elasticity modulus, water absorption and depth of penetration under varying curing conditions having produced concrete samples using Portland cement (PC), slag cement (SC) and limestone cement (LC). The samples were produced at 0.63 and 0.70 w/c (water/cement) ratios. Hardened concrete samples were then cured under three conditions, namely standard (W), open air (A) and sealed plastic bag (B). Although it was found that the early-age strength of slag cement was lower, it was improved significantly on 90th day. In terms of the effect of curing conditions on compressive strength, cure W offered the highest compressive strength, as expected, while cure A offered slightly lower compressive strength levels. An increase in the w/c ratio was found to have a negative impact on pozzolanic reactions, which resulted in poor hardened concrete properties. Furthermore, carbonation effect was found to have positive effects on some of the concrete properties, and it was observed to have improved the depth of water penetration. Moreover, it was possible to estimate the compressive strength with high precision using artificial neural networks (ANN). The values of the slopes of the regression lines for training, validating and testing datasets were 0.9881, 0.9885 and 0.9776, respectively. This indicates the high accuracy of the developed model as well as a good correlation between the predicted compressive strength values and the experimental (measured) ones.

**Keywords:** slag cement; portland limestone cement; curing; artificial neural networks; w/c

## 1. Introduction

Cement and concrete are two most commonly used construction materials in the world; however, the high level of $CO_2$ emissions associated with their production leads to major environmental issues. There are several studies focusing on the use of ground granulated blast-furnace slag, fly ash, silica fume and limestone in Portland cement as mineral admixtures in order to reduce these $CO_2$ emission levels. Limestone powder is widely used as a mineral admixture in concrete production thanks to its natural availability, and technical and economic advantages it has to offer [1].

There are a number of studies that reported increased compressive strength with the limestone addition, as it increases the early-age hydration ratio of Portland cement, which increases the compressive strength [2,3]. In addition, the Portland Cement Association explored the effects of hydration and setting time, heat evolution, microstructural properties and grain size distribution on the mechanical properties of PLC (Portland Limestone Cement) concrete. In terms of the hydration properties and compressive strength of paste and mortars produced using PLC, it was found that increasing the replacement level decreases compressive strength. However, this negative effect was reduced when finer ground limestone was used [1,4].

As the use of finer ground limestone powder results in increased nucleation area, it could be possible to accelerate the tri-calcium silicate ($C_3S$) reaction in Portland cement with the presence of limestone powder [5,6]. In other words, limestone surface plays an important role in increasing the area for nucleation in order to allow for the deposit of hydration products. The areas made available with limestone powder can reduce the energy barrier and they can accelerate the hydration product formation when compared to pore solution [7].

Nedhi et al. suggested that it is possible to produce more efficient and ecological cements without compromising on the cement properties with the use of pozzolanic industrial by-products in composite cements, as limestone is readily available in any cement manufacturing plant [8,9].

Slag cement is produced using ground granulated blast-furnace slag, a by-product of the steel industry. Blast-furnace slag is a binder material commonly used as an alternative to cement in concrete and clinker in cement. The use of slag cement in concrete production improves workability and allows for improved late-age strength, while offering several advantages, such as lower permeability and reduced carbon footprint. Slag cements are also used in high-strength concrete production [10]. Studies showed that the glassy phase content of slag has a significant impact on the strength of concrete. Escalante et al. showed that slag with 53.5% glassy fraction was more reactive than slag with 97% glassy fraction [11]. Wang et al. found that particle size of slag higher than 20 μm significantly increased the reactivity of the slag, while particle sizes lower than 5 μm played an important role in the hydration [12]. Nevertheless, a new method, dry granulation, was developed as an alternative to water quenching method used for blast-furnace slag [13].

Curing plays an important role in continued hydration of concrete. Particularly, early-age curing procedures have a direct impact on the late-age properties of concrete. Some of the recent studies focused on alternative curing methods. Curing is a treatment performed in order to improve the properties of hardened concrete, which is produced using hydraulic cement. Inefficient curing leads to significant losses in the long-term strength of the concrete and it may also result in the formation of micro-cracks and/or poor surfaces. Efficient curing conditions, on the other hand, contribute to improved concrete strength. Moreover, efficient curing conditions can improve the microstructure of the concrete and its wear resistance [14–16]. Water infiltration, chloride ion infiltration and gas infiltration in concrete are directly associated with porosity of the concrete and its pore properties. In this context, curing is very important if it is to reduce the porosity of the concrete. Mineral admixtures are among the factors contributing to the permeability of the concrete. However, it is recognized that the curing of concrete modified with mineral admixtures is more critical than that of the normal concrete [17–19]. Taşdemir explored the effect of mineral admixtures and curing conditions on the water absorption properties of the concrete and showed that the water absorption ratio varied based on the curing conditions used [20]. Sisomphon et al. showed the significance of a seven-day curing time in terms of the carbonation resistance of the mixes. Depth of carbonation of cement with fly ash or blast-furnace slag is significantly reduced when the curing time is extended between three to seven days [21]. Abdel-Hay applied three curing methods on the concrete produced using recycled aggregates, namely, air curing, moist curing and painted curing (Curassol-1). The author found that painted curing was very effective in improving the compressive strength of the concrete [22].

Artificial Intelligence (AI)-based techniques have been also widely used for prediction of the compressive strength and other mechanical properties of concrete mixtures [23–27]. The predication of concrete strength by integrating ultrasonic wave and artificial neural network (ANN) has been performed in some existing studies such as Trtnik et al. [28] and Kewalramani and Gupta [29].

In this study, concrete samples were produced using PC (Portland Cement), SC (Slag Cement) and LC (Portland Limestone Cement) cement with w/c (water/cement) ratios of 0.63 and 0.70, respectively. Concrete samples were then cured using three methods, namely, W, B and A, and their hardened concrete properties (compressive strength, ultrasonic pulse velocity, dynamic elasticity modulus, water absorption and depth of penetration) were explored. Using the data obtained from the experiment, an ANN model was developed and compressive strength estimations were made.

## 2. Materials and Methods

### 2.1. Materials

In this study, Portland limestone cement, blast-furnace slag added cement and Portland cement, all manufactured by the same plant, were used. The physical and chemical properties of the cements used are shown in Table 1.

**Table 1.** Chemical and Physical Properties of the Cements.

| CHEMICAL PROPERTIES | | | | | | | | | |
|---|---|---|---|---|---|---|---|---|---|
| Cement | CaO | $SiO_2$ | $Al_2O_3$ | $Fe_2O_3$ | MgO | $Na_2O$ | $K_2O$ | $SO_3$ | LOI |
| LC | 58.9 | 21.8 | 4.1 | 3.1 | 1.5 | 0.8 | 0.2 | 3.3 | 6.5 |
| PC | 64.2 | 19.1 | 4.9 | 2.8 | 2.0 | 1.1 | 0.4 | 3.9 | 1.8 |
| SC | 46.6 | 29.1 | 9.6 | 1.5 | 6.0 | 0.4 | 0.5 | 3.4 | 1.4 |

| PHYSICAL PROPERTIES | | | |
|---|---|---|---|
| Cement Type | PC (CEM I 42.5R) | LC (CEM II/A-L 42.5R) | SC (CEM III/B 42.5N) |
| Specific Weight | 3.15 | 2.90 | 3.05 |
| Blaine ($cm^2/g$) | 3200 | 5200 | 4900 |
| Initial Setting Time (min) | 110 | 150 | 230 |
| Final Setting Time (min) | 190 | 260 | 310 |

Two types of coarse-grained aggregate and one type of fine-grained aggregate were used in concrete production.

Coarse-grained (CA-1 and CA-2) and fine-grained (FA) aggregates complied with ASTM C 33 (Standard Specification for Concrete Aggregates) standard. Saturated surface dry (SSD) density of the coarse-grained aggregate was 2.59 $g/cm^3$ and the maximum particle size was 25 mm. Saturated surface dry (SSD) density of the fine-grained aggregate, on the other hand, was 2.62 $g/cm^3$. The fineness modulus of the fine aggregate was 2.6. The water absorption of the coarse aggregate was 2.50% and that of the fine aggregate was 2.75%. Poly (carboxylate ether)-based superplasticizer offering water reduction up to 30% was also used in the mix. Tap water from the Kastamonu water supply network was used in the curing and production of concrete samples.

### 2.2. Methods

Produced using varying w/c ratios and different cement types, concrete samples were subjected to compressive strength tests on the 3rd, 7th, 28th and 90th day. Concrete samples were produced with dimensions of 15 × 15 × 15 cm for the compressive strength test. The w/c ratios of concrete samples were 0.63 and 0.70. Fresh concrete was placed in two equal layers and each layer was rod 25 times. Concrete samples were taken out of the molds after 24 h and the curing procedure started. Three curing methods were used. The first method (W) involved water curing of the samples until the test day; the second method (B) involved curing in a sealed plastic bag; and the third method (A) involved curing in open air. The plastic bag curing was chosen to reduce the moisture content (to reduce the effect of evaporation) in the concrete. Three samples were produced for each one of the test days. A total number of six mixes and 216 concrete samples were produced as part of the experimental study. Variables of the experimental study are given in Table 2.

**Table 2.** Variables of the experimental study.

| | Factor 1 | Factor 2 | Factor 3 |
|---|---|---|---|
| Cement Type | PC | LC | SC |
| w/c Ratio | 0.63 | 0.70 | |
| Curing Conditions | Water (W) | Plastic Bag (B) | Air (A) |

Cement dosage was kept constant at 300 kg/m$^3$ in the mix and the water ratio was altered. Superplasticizer (SP) was used at a ratio of 1% by volume of cement. Amounts of materials used in the concrete mix are shown in Table 3.

**Table 3.** Amounts of materials used in the concrete mix (kg/m$^3$).

| Mix No. | Cement Type | w/c | Cement | Water | FA | CA-1 | CA-2 | SP |
|---|---|---|---|---|---|---|---|---|
| 1 | PC | 0.63 | 300 | 189 | 638 | 456 | 730 | 3 |
| 2 | PC | 0.70 | 300 | 210 | 617 | 441 | 705 | 3 |
| 3 | LC | 0.63 | 300 | 189 | 631 | 451 | 721 | 3 |
| 4 | LC | 0.70 | 300 | 210 | 610 | 435 | 697 | 3 |
| 5 | SC | 0.63 | 300 | 189 | 636 | 454 | 726 | 3 |
| 6 | SC | 0.70 | 300 | 210 | 614 | 439 | 702 | 3 |

Ultrasonic pulse velocity (UPV) of the hardened concrete samples was measured in compliance with ASTM C 597 standard. Travel time of ultrasonic pulse was measured using probes on two surfaces and ultrasound gel was used for optimal contact. UPV values were calculated using Equation (1):

$$v = \frac{s}{t} \cdot 10^6 \tag{1}$$

Here;

$v$: Ultrasonic pulse velocity (m/sec)
$s$: Distance between transmitter and receiver probes (m)
$t$: Time (μsec)

Ideally, this modulus is measured directly on concrete samples under compression by recording the load-deformation curve. However, this is not always easy. To avoid demanding and time-consuming direct measurements of elastic modulus ($E_c$), simplified approaches with either a theoretical or an empirical basis have been developed. Non-destructive tests take into account the acoustic impedance of the system components—important factors influencing ultrasonic wave propagation. The dynamic elastic modulus was determined by measuring the pulse velocity along the composite and using electrical transducers located on the opposite sides of the cubic specimens of concrete. The energy supplied by the ultrasound depends on how compact the composite is, including the void presence and the void sizes [30]. $E_d$ values of the concrete samples were calculated using Equation (2). The Poisson's ratio ($\mu$) of the concrete was 0.20 (estimated value) in the experimental study. Densities of the concrete samples were determined experimentally according to ASTM C 642-13 standard. Densities of the concrete samples ($\rho$) were found in a range between 2.35 and 2.45.

$$E_d = \frac{V^2 \cdot p \cdot (1+\mu) \cdot (1-2\mu)}{(1-\mu)} \tag{2}$$

$E_d$: Dynamic elasticity modulus (MPa)
$V$: Ultrasonic pulse velocity (m/sec)
$\rho$: Density
$\mu$: Poisson's Ratio

Water penetration depth of concrete samples was measured using a water permeability test. TS EN 12390-8 (Depth of penetration of water under pressure) standard was used in the measurement for water permeability value of the concrete samples. Concrete samples were fixed safely in the mechanism with plastic gaskets placed under the samples in order to prevent any leaks under pressure. As part of the experiment, concrete samples were subjected to 5 bars of pressure for 72 ± 2 h. After 72 h, the samples were removed from the mechanism and they were subjected to splitting tensile strength test. Split into two, concrete samples were measured for water penetration depth using a digital gauge. Water absorption ratio of concrete was measured using cubic samples of 100 × 100 × 100 mm in size. Concrete samples were subjected to water absorption test at the end of curing times. ASTM C 642 standard was used in order to measure the water absorption ratio of the concrete samples. Samples were dried in accordance with ASTM C 642 standard and they were weighed accordingly. After the measurements were taken, samples were left in water for 24 h. Saturated surface dry (SSD) weights of the samples were measured after 24 h.

## 3. Results and Discussion

### 3.1. Effect of Cement Type on Hardened Concrete Properties

Figure 1 shows the compressive strength of concrete samples, produced using different types of cements, over time.

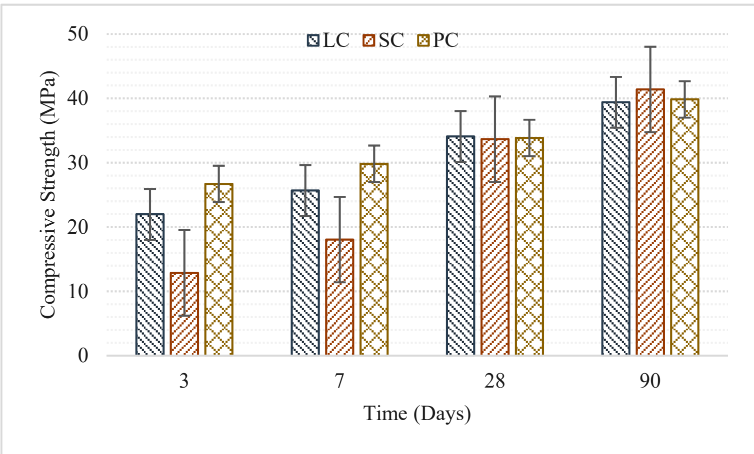


**Figure 1.** Effect of cement type on the compressive strength of concrete.

Figure 1 shows that three-day and seven-day compressive strengths of concrete samples produced using SC cement with the lowest clinker ratio was approximately 20 MPa. 28-days compressive strengths of concrete samples produced using SC cement were not significantly different from the other concrete types. As pozzolanic reactions take place by the 90th day, the compressive strength of the concrete samples produced using SC cement was approximately 50 MPa. Three-day and seven-day compressive strengths of concrete samples produced using LC cement were lower than that of the concrete samples produced using PC cement. Approximately 10% strength loss was observed in early-age strength of the concrete samples due to the decreased clinker ratio used. However, this loss was eliminated on the 28th and 90th day and it was found that concrete samples produced using PC and LC cements had similar properties. Although limestone does not offer pozzolanic properties, it offers the same performance as PC cement due to nucleation's contribution to hydration and acts as a filler. Concrete samples produced using PC, i.e., the reference cement, offered high compressive strengths on all the testing days. Compressive strengths of all the concrete samples increased with the increase in curing time.

Figure 2 shows the effect of cement type on some hardened concrete properties. As shown in Figure 2a, UPV values increased with the increased curing time. UPV values increased as compressive strengths of concrete samples increased. Three-day and seven-day UPV values of concrete samples produced using SC cement were in the range of 4.10–4.41 km/sec. UPV values of concrete samples produced using SC cement was equal to those of the concrete samples produced using PC cement when the curing time was increased. UPV values of concrete samples produced using LC and PC cements offered similar properties up to the 28th day (4.40–4.80 km/sec). On the 90th day, pozzolanic reactions in SC cement played a role in the increasing UPV values. Figure 2b shows the change in dynamic elasticity modulus ($E_d$) due to cement type. The three-day $E_d$ value of the concrete samples produced using SC cement was 41,455 MPa, while this value was increased by 35.9% on the 90th day to add up to 56,366 MPa. Such an increase in $E_d$ value can be accounted for by the improved microstructure thanks to pozzolanic reactions, which has a positive impact on the compressive strength. $E_d$ values of both LC and PC cements increased with an increased curing time. The differences between the $E_d$ properties of LC and PC cements were not significant on the 28th and 90th day. Figure 2c shows the water absorption ratios of concrete samples produced using different cement types over time. Water absorption ratios of concrete samples produced using LC and PC cements after three days of curing were approximately 5.6%. However, water absorption ratios of concrete samples produced using LC and PC cements after 90 days of curing were approximately 4.7%. Water absorption ratios of concrete samples produced using SC cement were lower than those of concrete samples produced using LC and PC cements. The water absorption ratio of concrete samples produced using SC cement was approximately 3.80%. Figure 2d shows the water penetration depths of concrete samples produced using different types of cements. Increased curing time resulted in decreased water penetration depth. Water penetration depths of concrete samples produced using SC and LC cements were similar on the 28th and 90th day. The fact that LC and SC cements had higher Blaine fineness values reduced the water penetration depth.

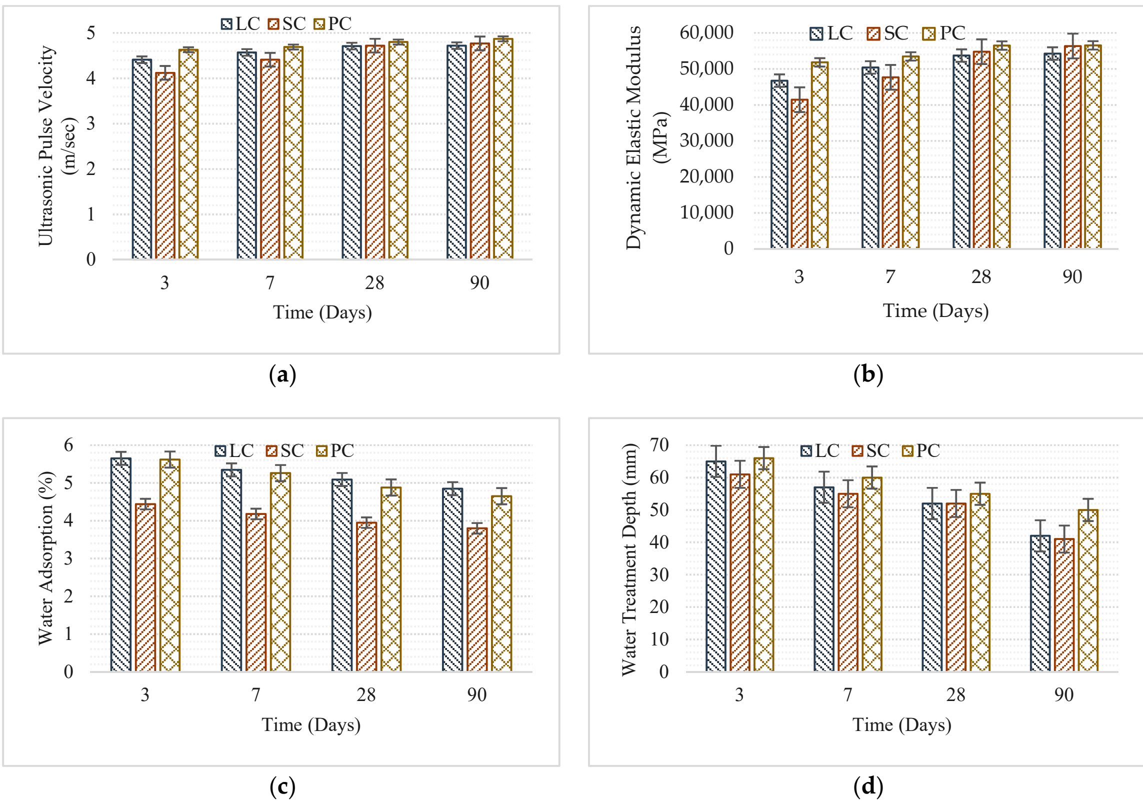


**Figure 2.** Effect of cement type on some hardened concrete properties. (**a**) Ultrasonic Pulse Velocity; (**b**) Dynamic Elastic Modulus; (**c**) Water Adsorption; (**d**) Water Treatment Depth.

Although the early-age compressive strength (3–7 days) of SC cement including blast-furnace slag was low, its 90-days compressive strength was higher. This finding was also evident from UPV and $E_d$ values. Moreover, increasing the curing time of concrete samples produced using SC cement was found to reduce the water penetration depth. Considering the low clinker content, pozzolanic reactions played a positive role in the improved late-age compressive strength of concrete. LC cement, which was produced using limestone, generally offered properties similar to PC cement. LC cement performed similar to SC cement only in terms of water penetration depth. It was observed that cement fineness is an important parameter in water penetration depth.

### *3.2. Effect of w/c (Water/Cement) Ratio on Compressive Strength*

Figure 3 shows the compressive strength of concrete produced using different w/c ratios over time. As shown in Figure 3, decreased w/c ratio results in increased compressive strength at all testing days. Compressive strength is reduced by 26.5% and 21.1%, respectively, on the third and seventh day as a result of the increase in w/c ratio from 0.63 to 0.70. The same ratio was found to be 19.4% on the 28th day. Although the loss in compressive strength due to w/c ratios was reduced up to the 28th day, the loss in compressive strength on the 90th day was found to be 24.9%. This significant difference between w/c ratios can be accounted for by the pozzolanic reactions. Moreover, very high w/c ratios had a negative impact on the pozzolanic reactions.

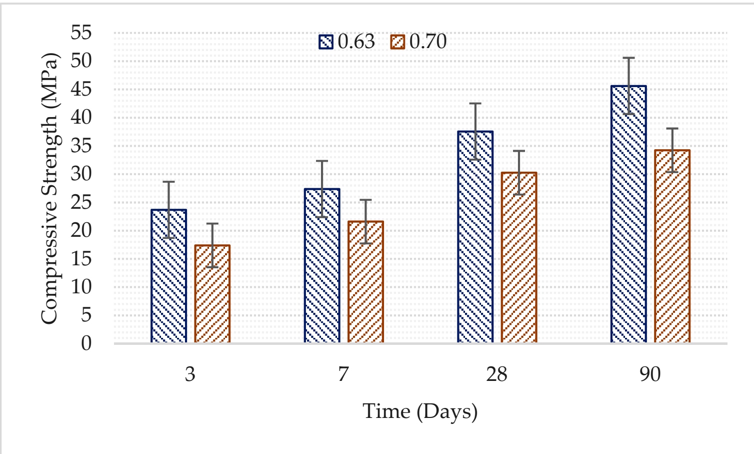


**Figure 3.** Effect of w/c ratio on the compressive strength of concrete.

Figure 4 shows some hardened concrete properties of the concretes produced using different w/c ratios. As expected, the experiment results showed that decreasing the w/c ratio increased UPV and $E_d$ values (Figure 4a,b). Nevertheless, decreasing the w/c ratio also decreased water absorption and water penetration depth (Figure 4c,d). It was observed that the water penetration depth was reduced to 40 mm in concrete samples produced using a w/c ratio of 0.63, while this value was 50 mm in concrete samples produced using a w/c ratio of 0.70. The change in w/c ratio did not have a significant effect on UPV. The difference between UPV values was reduced, especially with the increasing curing times.

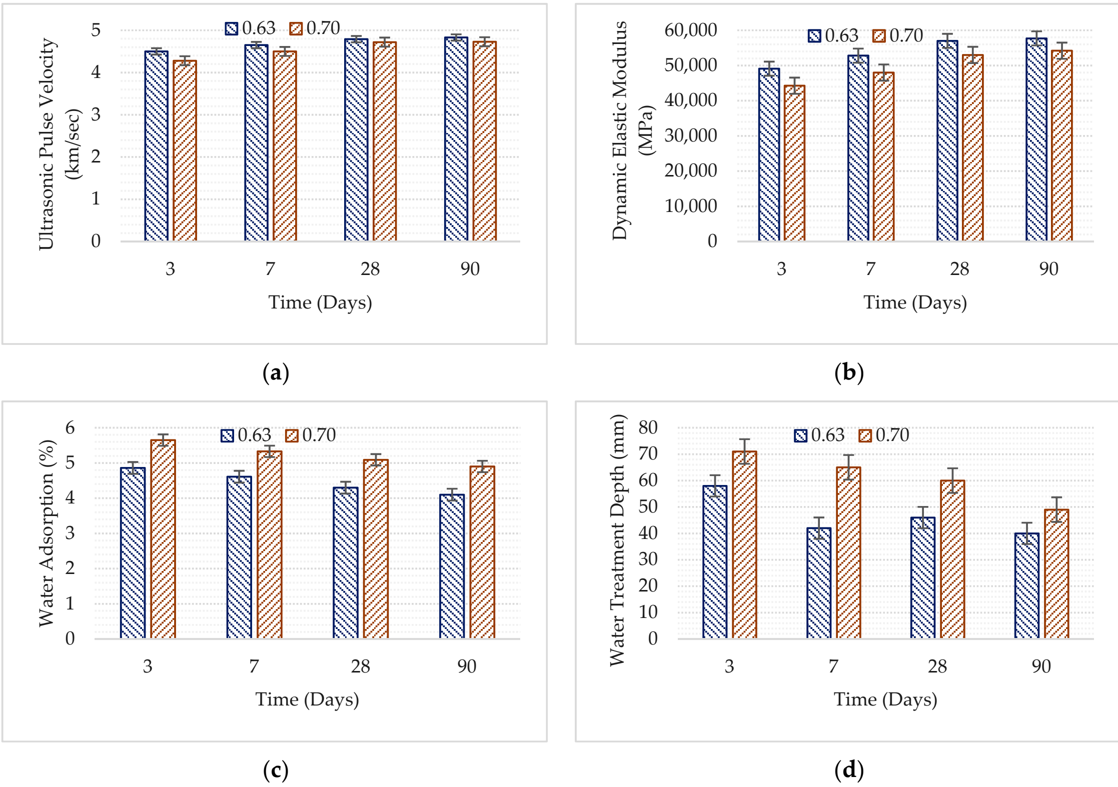


**Figure 4.** Effect of w/c ratio on some hardened concrete properties. (**a**) Ultrasonic Pulse Velocity; (**b**) Dynamic Elastic Modulus; (**c**) Water Adsorption; (**d**) Water Treatment Depth.

### *3.3. Effects of Curing Conditions on Compressive Strength*

Figure 5 shows the change in compressive strength over time due to varying curing conditions used. As shown in Figure 5, the concrete samples cured in water consistently offered higher compressive strength values for all testing days. Three-day compressive strengths of the samples cured in water and in a plastic bag were above 25 MPa. However, three-day compressive strengths of the samples cured in open air were below 25 MPa. Concrete samples cured in open air were able to reach at 25 MPa only on the seventh day. A closer look at 28-days compressive strength showed that samples cured in water and in a plastic bag did not have significant differences. However, the compressive strength of samples cured in open air was reduced by 10%. The compressive strength of samples cured in open air was approximately 12% lower than that of the water cured samples on the 90th day.

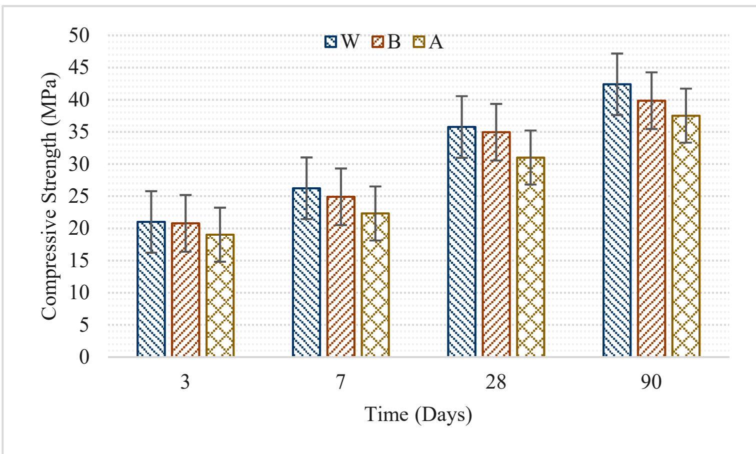


**Figure 5.** Effect of curing conditions on the compressive strength of concrete over time.

The effect of vaporization was limited for the samples cured in plastic bags and the moisture loss was reduced. Due to this effect, the samples cured in plastic bags offered similar behaviors to those cured in water. Compressive strengths of the samples cured in open air was lower than those of the other samples; however, these results were improved on the 90th day. It is believed that pozzolanic reactions play a role in this result as such reactions continue to take place with humidity in the air.

Figure 6a shows the effect of different curing conditions on UPV values. As it was the case in compressive strength, continuous water curing contributed to hydration, which in return increased UPV values over time. UPV value of the concrete samples cured in water was 4.9 km/sec on the 90th day. UPV value of the concrete samples cured in air, on the other hand, was 4.7 km/sec on the 90th day. Similar results were observed in Figure 6b for $E_d$ values. The prevention of moisture loss in concrete samples allowed for a continued hydration and resulted in increased $E_d$ values. Moisture loss prevention of the samples cured in plastic bags was an indicator of this finding. It was found that UPV and $E_d$ values on the 90th day measured for the samples cured in air and in plastic bags were similar. The reason behind the reduced loss of compressive strength in samples cured in air is believed to be the carbonation reactions taking place. Water molecules formed after carbonation contributes to the hydration. Equation (3) is the equation for the carbonation reaction.

$$Ca(OH)_2 + CO_2 \rightarrow CaCO_3 + H_2O \tag{3}$$

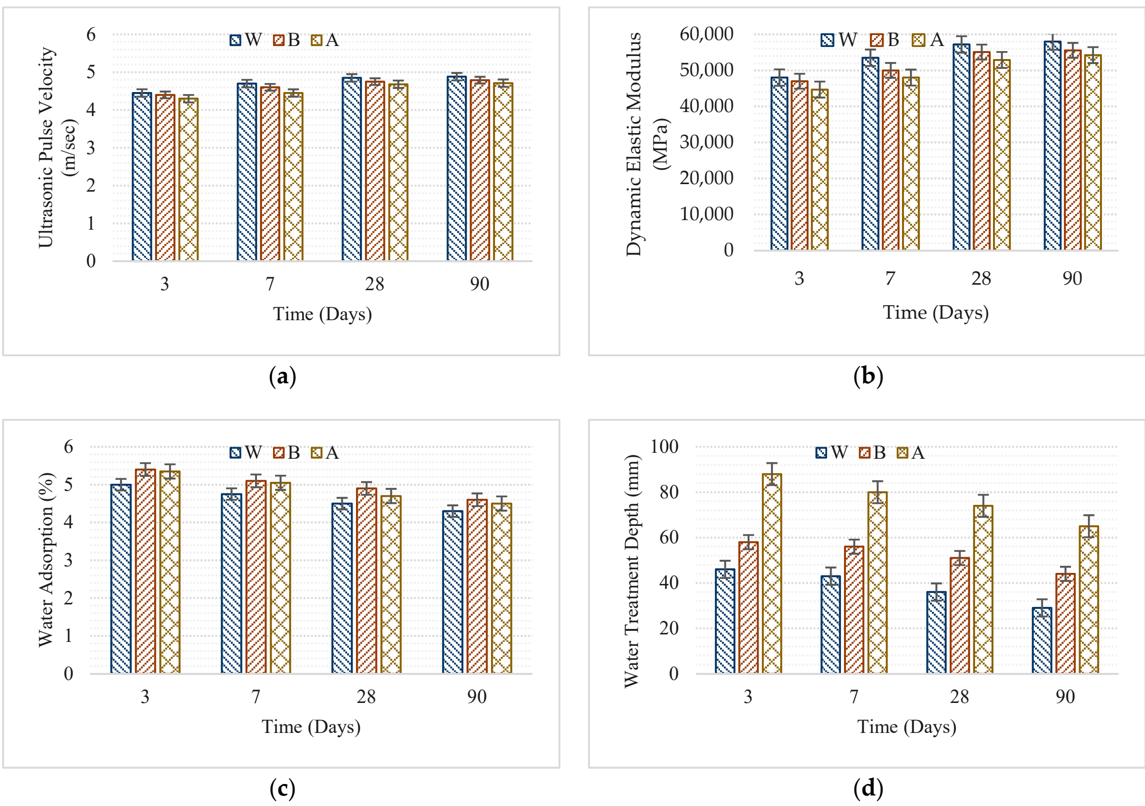


**Figure 6.** Effect of curing conditions on some hardened concrete properties. (**a**) Ultrasonic Pulse Velocity; (**b**) Dynamic Elastic Modulus; (**c**) Water Adsorption; (**d**) Water Treatment Depth.

Although the water absorption ratios of samples cured in air and in plastic bags were higher than those of the samples cured in water, an approximate 0.25% difference was found between the samples (Figure 6c). The reason behind this insignificant difference between water absorption ratios is believed to be the carbonation reaction. However, this effect was not observed in the water penetration depth as shown in Figure 6d. Water penetration depth of the samples cured in air was 65 mm on the 90th day, while it was 29 mm for those cured in water. The positive effect of carbonation was eliminated in the presence of the pressure water effect.

### *3.4. The Use of Feed-Forward Neural Network with Backpropagation*

In this study, a feed-forward neural network with backpropagation model was developed in order to estimate the compressive strength, one of the most important mechanical properties of concrete. Data obtained from a total number of 72 concrete mixes, experimentally produced, was used in the modeling. 50 of these experimental data were used to train the model, 11 were used to test the model and the remaining 11 were used to confirm the model. As input and output parameters of the ANN model have different units, these values were normalized using the following formula: $X' = 0.8^{*} (X_i - X_{min})/(X_{max} - X_{min}) + 0.1$. Here, X′ is the normalized data, $X_i$ is the input value and $X_{max}$ and $X_{min}$ are maximum and minimum values in the input set. A backpropagation algorithm was used to train the ANN. Moreover, logarithmic sigmoid activation function was selected as the transfer function. The ANN model developed for this study was tried for different layers and neuron counts. The number of iterations for each model was limited to 1000 in detection of the best ANN model. As a result, the network architecture including a hidden layer and eight neurons were found to give the best result for compressive strength estimation among other ANN models. Figure 7 shows the artificial network architecture.

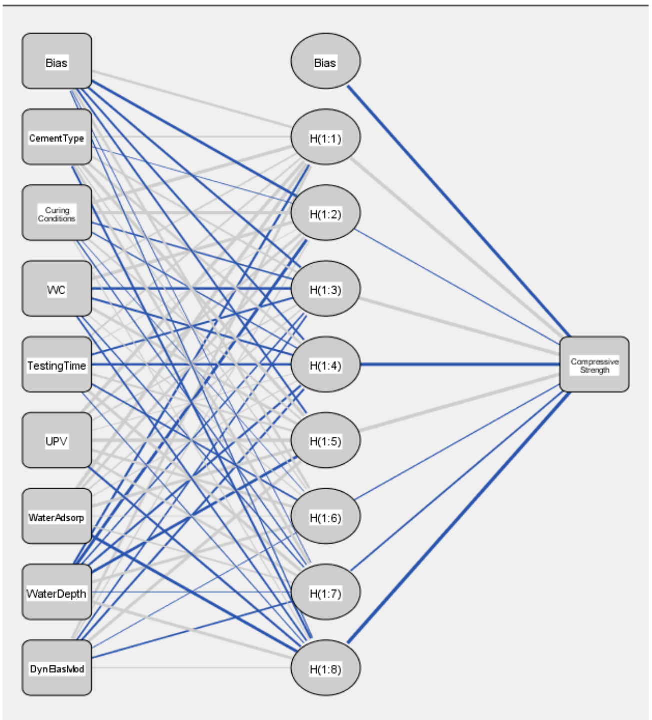


**Figure 7.** Architecture of artificial neural networks (ANN) model.

At the end of the ANN training, the mean squared error of the compressive strength estimation was found to be $2.2389 \times 10^{-4}$. Figure 8 shows the regression values obtained at the end of the ANN training.

The ANN model versus the experimental results for training, validating and testing datasets are shown in Figure 8. The closer to the value of the slope of the regression line for predicted versus the measured values is to 1, the more accurate is the model. It can be seen that the values of the slopes of the regression lines for training, validating and testing datasets are 0.9881, 0.9885 and 0.9776, respectively. This indicates the high accuracy of the developed model as well as a good correlation between the predicted compressive strength values and the experimental (measured) ones.

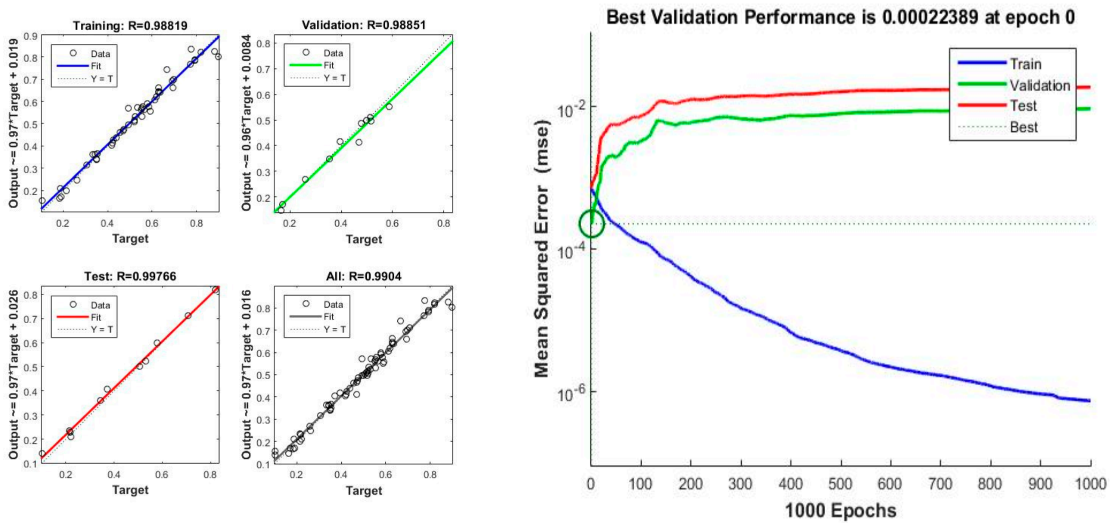


(**a**) (**b**)

**Figure 8.** Regression values for the ANN model. (**a**) Regression Values; (**b**) MSE Values.

Forty mixes were selected in order to create a simulation of the ANN model developed and model's ability to estimate was explored. As shown in Figure 9, the model was quite successful in estimating the compressive strength values. This is a further confirmation of the fact that the ANN structure was modeled smoothly. The values of the error measures (RMSE-Root Mean Squares of Error and MAE-Mean absolute error) of this model for training, validating and testing datasets are given in Table 4.

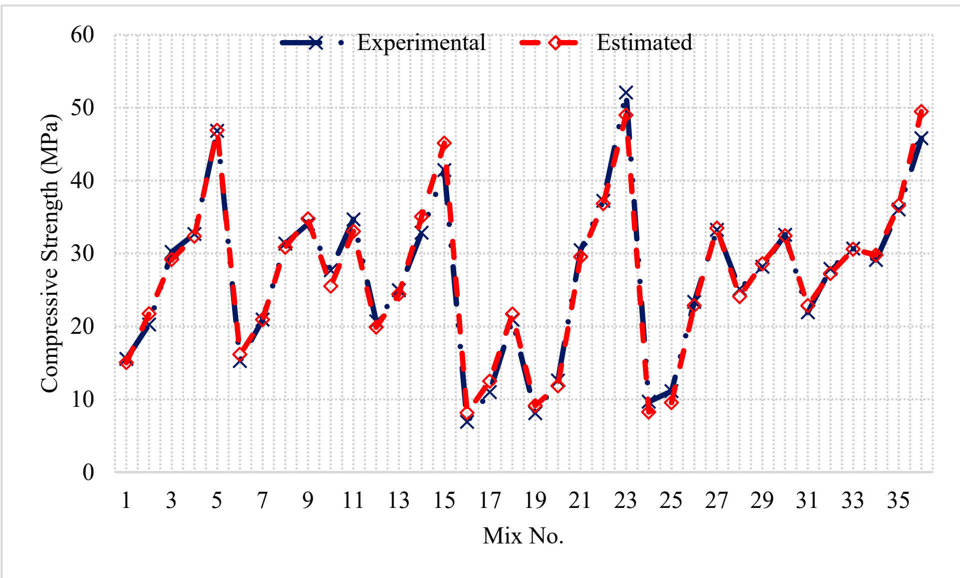


**Figure 9.** A comparison of the experimental and estimated compressive strength values.

**Table 4.** Error measures of the 40 selected ANN models.

| **Training Data** | | | **Validating Data** | | |
| --- | --- | --- | --- | --- | --- |
| RMSE (MPa) | MAE (MPa) | $R^2$ | RMSE (MPa) | MAE (MPa) | $R^2$ |
| 6.69 | 4.82 | 0.987 | 6.12 | 4.27 | 0.988 |
| **Testing Data** | | | **All Data** | | |
| RMSE (MPa) | MAE (MPa) | $R^2$ | RMSE (MPa) | MAE (MPa) | $R^2$ |
| 6.58 | 4.46 | 0.992 | 6.40 | 4.85 | 0.993 |

## 4. Results

1. Due to its slag content, LC cement showed lower compressive strength on the third and seventh day. However, there were no significant differences observed between cements when the curing time was increased. It was further confirmed that the curing process and time must be kept under check for slag cement as it offers pozzolanic properties.
2. In terms of early-age strength, PC samples gave higher compressive strength values. Nevertheless, increasing the curing time eliminated significant differences between cement samples (especially on the 90th day).
3. As reported in the literature, increasing the w/c ratio reduces the compressive strength. Notwithstanding, the compressive strength of the concrete mix produced using a w/c ratio of 0.70 was 30 MPa. This effect is made possible with the finer grain size of modern cements and the use of superplasticizers.
4. There were no significant differences between curing conditions. In terms of curing conditions, hardened concrete properties can be sorted as W>B>A by performance. As fine ground cement had a positive impact on the hydration level, there were no significant differences between the samples in terms of curing conditions.
5. Increasing the fineness of the cement plays an important role in water penetration depth. Moreover, the increase in w/c ratios had a negative impact on the pozzolanic reactions. Especially the hardened concrete properties of the samples produced using slag cement were adversely affected by the increased w/c ratio.
6. Thanks to the carbonation effect, the compressive strength loss of samples cured in air was reduced. Additionally, carbonation reduced the losses in UPV and $E_d$ values. However, there was no positive impact of carbonation found in the permeability test performed under pressure.
7. The ANN model developed in this study makes it possible to estimate the changes in compressive strength due to cement type, w/c ratio, curing conditions, curing time, UPV, $E_d$, water absorption and water penetration depth. This ANN model offers a nondestructive method for compressive strength using the material properties.

**Author Contributions:** H.Y. and S.M. conceived and designed the experiments; A.A. performed the experiments; S.M. analysed the data; G.K. and H.Y. wrote the paper.

**Funding:** This research received no external funding.

**Conflicts of Interest:** The authors declare no conflict of interest.

## References

1. Moon, G.D.; Oh, S.; Jung, S.H.; Choi, Y.C. Effects of the fineness of limestone powder and cement on the hydration and strength development of PLC concrete. *Constr. Build. Mater.* **2017**, *135*, 129–136. [CrossRef]
2. Marzouki, A.; Lecomte, A.; Beddey, A.; Diliberto, C.; Ouezdou, M.B. The effects of grinding on the properties of Portland-limestone cement. *Constr. Build. Mater.* **2013**, *48*, 1145–1155. [CrossRef]
3. Lothenbach, B.; Le Saout, G.; Gallucci, E.; Scrivener, K. Influence of limestone on the hydration of Portland cements. *Cem. Concr. Res.* **2008**, *38*, 848–860. [CrossRef]
4. Aqel, M.; Panesar, D.K. Hydration kinetics and compressive strength of steam-cured cement pastes and mortars containing limestone filler. *Constr. Build. Mater.* **2016**, *113*, 359–368. [CrossRef]
5. Tsivilis, S.; Batis, G.; Chaniotakis, E.; Grigoriadis, G.; Theodossis, D. Properties and behavior of limestone cement concrete and mortar. *Cem. Concr. Res.* **2000**, *30*, 1679–1683. [CrossRef]
6. Zelić, J.; Krstulović, R.; Tkalčec, E.; Krolo, P. Durability of the hydrated limestone-silica fume Portland cement mortars under sulphate attack. *Cem. Concr. Res.* **1999**, *29*, 819–826. [CrossRef]

7. Guemmadi, Z.; Houari, H.; Resheidat, M.; Toumi, B. Better Use of Limestone Filler in Concrete. In Proceedings of the International Conference on Construction and Building Technology, ICCBT, Kuala Lumpur, Malaysia, 16–20 June 2008.
8. Nehdi, M.; Mindess, S.; Aïtcin, P.C. Optimization of high strength limestone filler cement mortars. *Cem. Concr. Res.* **1996**, *26*, 883–893. [CrossRef]
9. de Sensale, G.R.; Viacava, I.R. A study on blended Portland cements containing residual rice husk ash and limestone filler. *Constr. Build. Mater.* **2018**, *166*, 873–888. [CrossRef]
10. Liu, Z.; El-Tawil, S.; Hansen, W.; Wang, F. Effect of slag cement on the properties of ultra-high performance concrete. *Constr. Build. Mater.* **2018**, *190*, 830–837. [CrossRef]
11. Escalante, J.I.; Gómez, L.Y.; Johal, K.K.; Mendoza, G.; Mancha, H.; Méndez, J. Reactivity of blast-furnace slag in Portland cement blends hydrated under different conditions. *Cem. Concr. Res.* **2001**, *31*, 1403–1409. [CrossRef]
12. Wang, P.Z.; Trettin, R.; Rudert, V. Effect of fineness and particle size distribution of granulated blast-furnace slag on the hydraulic reactivity in cement systems. *Thermochim. Acta* **2004**, *17*, 161–167. [CrossRef]
13. Liu, J.; Yu, Q.; Zuo, Z.; Yang, F.; Duan, W.; Qin, Q. Blast furnace slag obtained from dry granulation method as a component in slag cement. *Constr. Build. Mater.* **2017**, *131*, 381–387. [CrossRef]
14. Liu, B.; Luo, G.; Xie, Y. Effect of curing conditions on the permeability of concrete with high volume mineral admixtures. *Constr. Build. Mater.* **2018**, *167*, 359–371. [CrossRef]
15. Ramezanianpour, A.A.; Malhotra, V.M. Effect of curing on the compressive strength, resistance to chloride-ion penetration and porosity of concretes incorporating slag, fly ash or silica fume. *Cem. Concr. Compos.* **1995**, *17*, 125–133. [CrossRef]
16. Güneyisi, E.; Gesoğlu, M.; Özturan, T.; Özbay, E. Estimation of chloride permeability of concretes by empirical modeling: Considering effects of cement type, curing condition and age. *Constr. Build. Mater.* **2009**, *23*, 469–481. [CrossRef]
17. Sajedi, F.; Razak, H.A.; Mahmud, H.B.; Shafigh, P. Relationships between compressive strength of cement-slag mortars under air and water curing regimes. *Constr. Build. Mater.* **2012**, *31*, 188–196. [CrossRef]
18. Ahari, R.S.; Erdem, T.K.; Ramyar, K. Thixotropy and structural breakdown properties of self consolidating concrete containing various supplementary cementitious materials. *Cem. Concr. Compos.* **2015**, *59*, 26–37. [CrossRef]
19. Atiş, C.D. Strength properties of high-volume fly ash roller compacted and workable concrete, and influence of curing condition. *Cem. Concr. Res.* **2005**, *35*, 1112–1121. [CrossRef]
20. Tasdemir, C. Combined effects of mineral admixtures and curing conditions on the sorptivity coefficient of concrete. *Cem. Concr. Res.* **2003**, *33*, 1637–1642. [CrossRef]
21. Sisomphon, K.; Franke, L. Carbonation rates of concretes containing high volume of pozzolanic materials. *Cem. Concr. Res.* **2007**, *37*, 1647–1653. [CrossRef]
22. Abdel-Hay, A.S. Properties of recycled concrete aggregate under different curing conditions. *HBRC J.* **2017**, *13*, 271–276. [CrossRef]
23. Bui, D.K.; Nguyen, T.; Chou, J.S.; Nguyen-Xuan, H.; Ngo, T.D. A modified firefly algorithm-artificial neural network expert system for predicting compressive and tensile strength of high-performance concrete. *Constr. Build. Mater.* **2018**, *180*, 320–333. [CrossRef]
24. Behnood, A.; Behnood, V.; Gharehveran, M.M.; Alyamac, K.E. Prediction of the compressive strength of normal and high-performance concretes using M5P model tree algorithm. *Constr. Build. Mater.* **2017**, *142*, 199–207. [CrossRef]
25. Golafshani, E.M.; Behnood, A. Application of soft computing methods for predicting the elastic modulus of recycled aggregate concrete. *J. Clean. Prod.* **2018**, *176*, 1163–1176. [CrossRef]
26. Atici, U. Prediction of the strength of mineral admixture concrete using multivariable regression analysis and an artificial neural network. *Expert Syst. Appl.* **2011**, *38*, 9609–9618. [CrossRef]
27. Behnood, A.; Golafshani, E.M. Predicting the compressive strength of silica fume concrete using hybrid artificial neural network with multi-objective grey wolves. *J. Clean. Prod.* **2018**, *202*, 54–64. [CrossRef]

28. Trtnik, G.; Kavčič, F.; Turk, G. Prediction of concrete strength using ultrasonic pulse velocity and artificial neural networks. *Ultrasonics* **2009**, *49*, 53–60. [CrossRef]
29. Kewalramani, M.A.; Gupta, R. Concrete compressive strength prediction using ultrasonic pulse velocity through artificial neural networks. *Autom. Constr.* **2006**, *15*, 374–379. [CrossRef]
30. Gencel, O.; Brostow, W.; Martinez-Barrera, G.; Gok, M.S. Mechanical properties of polymer concretes containing different amount of hematite or colemanite. *Polimery/Polymers* **2012**, *57*, 277.